Inhibition of strigolactone receptors by *N*-phenylanthranilic acid derivatives: structural and functional insights

Cyril Hamiaux[‡1], Revel S. M. Drummond[‡], Zhiwei Luo[‡], Hui Wen Lee[‡,§], Prachi Sharma[‡,§], Bart J. Janssen[‡], Nigel B. Perry[¶,#], William A. Denny[&], Kimberley C. Snowden[‡2]

Supporting Information

List of content:

Supplementary Tables

Atom numbering in strigolactone compounds	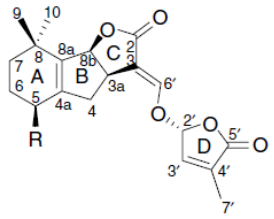

Name	Chiral centres				Structure	Source
	3a	-	8b	2’		
(rac)-GR24	R*	-	S*	R*	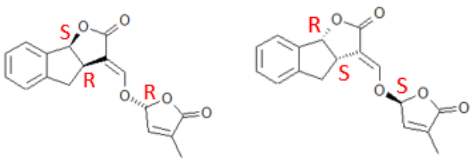	Chiralix
(+)-GR24	R	-	S	R	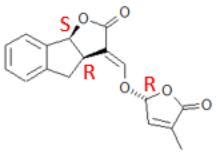	Chiralix

Name	Chiral centres				Structure	Source
	3a	5	8b	2’		
(rac)-Strigol	R*	S*	S*	R*	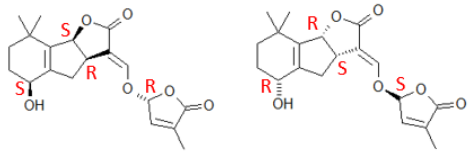	OlChemlm

Name	Chiral centres				Structure	Source
	3a	4	8b	2’		
(rac)-Orobanchol	R*	R*	R*	R*	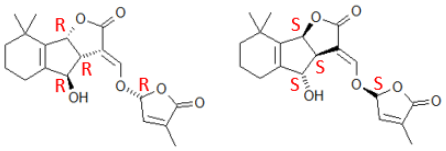	OlChemlm

Name	Chiral centres				Structure	Source
	3a	-	8b	2’		
(rac)-5DS	R*	-	S*	R*	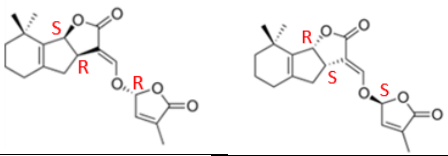	OlChemlm
(+)-5DS	R	-	S	R	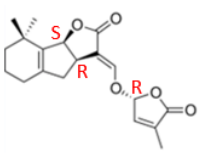	Wageningen University

(-)-5DS	S	-	R	S	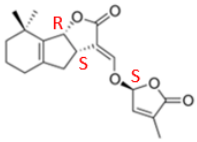	Wageningen University
(+)-2'-*epi*-5DS	R	-	S	S	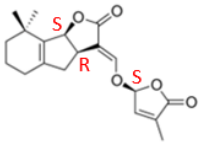	Wageningen University
(-)-2'-*epi*-5DS	S	-	R	R	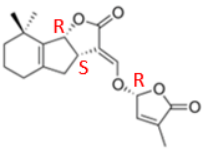	Wageningen University

Table S1. Strigolactone compounds used in this study. The 5DS pure isomers were a kind gift from Harro Bouwmeester and Yanxia Zhang (Wageningen University)

Protein		Tolfenamic acid	MNAB	Mefenamic Acid	Flufenamic acid	(rac)-GR24	(+)-GR24	YLG
DAD2	K_d (μM)	4.3 ± 0.5	4.6 ± 0.5	4.7 ± 0.5	10.8 ± 0.5	31.6 ± 6.9	28.1 ± 6.5	n.d.
	K_i (μM)	0.12 ± 0.02	0.16 ± 0.02	0.39 ± 0.08	n.d.	n.d.	n.d.	-
	$K_{1/2}$ (μM)	1.06 ± 0.08	1.32 ± 0.09	1.28 ± 0.11	n.d.	n.d.	n.d.	1.12 ± 0.10
	k_{cat} (min^{-1})	-	-	-	-	-	-	0.076 ± 0.003
OsD14	K_d (μM)	9.3 ± 0.4	8.0 ± 0.4			44 ± 26		n.d.
	K_i (μM)	3.20 ± 0.54	2.40 ± 0.42			n.d.		-
	$K_{1/2}$ (μM)	3.42 ± 0.26	3.35 ± 0.27			n.d.		3.32 ± 0.36
	k_{cat} (min^{-1})	-	-			-		0.150 ± 0.008
AtD14	K_d (μM)	11.2 ± 0.7	11.0 ± 0.6			37 ± 14		n.d.
	K_i (μM)	2.52 ± 0.27	1.90 ± 0.25			n.d.		-
	$K_{1/2}$ (μM)	1.02 ± 0.05	1.21 ± 0.11			n.d.		1.05 ± 0.08
	k_{cat} (min^{-1})	-	-			-		0.102 ± 0.003

Table S2. Binding and kinetic parameters of DAD2, OsD14 and AtD14 with substrates and inhibitors

Compounds B1-B118 are N-Phenylanthranilic acid derivatives			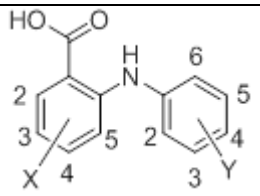	
Compound ID	X	Y	formula	MW
B1	3-Br, 4-F	4-I, 6-F	C13H6BrF2IN2O4	499.00
B2	3-Br, 4,5- =NON=	4-I, 6-F	C13H6BrFIN3O3	478.18
B3	3,4-diF, 5-NO_2	4-I, 6-F	C13H6F3IN2O4	438.10
B4	4.5-diF	2,6-diF	C13H6F4INO2	411.09
B5	5-NO_2	2,6-diF	C13H8F2N2O4	294.22
B6	4-Br	3-Br	C13H9Br2NO2	371.03
B7	4-Cl	3-Cl	C13H9Cl2NO2	282.13
B8	4-I	3-I	C13H9I2NO2	465.03
B9	H	3-Cl	C13H10ClNO2	247.68
B10	4-Br	H	C13H10BrNO2	292.13
B11	H	3-F	C13H10FNO2	231.23
B12	H	2-F	C13H10FNO2	231.23
B13	H	2-Cl	C13H10ClNO2	247.68
B14	H	4-Cl	C13H10ClNO2	247.68
B15	3-aza	2-CO_2H	C13H10N2O4	258.23
B16	H	2-SO_3H	C13H11NO5S	293.30
B17	3-NO_2, 4-NH_2	H	C13H11N3O4	273.30
B18	4-NO_2	4-NH_2	C13H11N3O4	273.50
B19	H	2-NH_2	C13H12N2O2	228.25
B20	H	2-SO_2NH_2	C13H12N2O4S	292.31
B21	5-CO_2H	4-F	C14H10FNO4	275.24
B22	5-CO_2H	2-I	C14H10INO4	383.14
B23	5-CO_2H	2-Br	C14H10BrNO4	336.14
B24	5-CO_2H	2-F	C14H10FNO4	275.24
B25	5-CO_2H	3-NO_2	C14H10N2O6	302.25
B26	5-CO_2H	4-NO_2	C14H10N2O6	302.25
B27	5-CO_2H	4-Cl	C14H10ClNO4	291.69
B28	H	3-CF_3	C14H10F3NO2	281.20
B29	5-CO_2H	4-Br	C14H10BrNO4	336.14
B30	2-NO_2, 4-F	2,6-diI	C14H10FIN2O4	416.15

B31	4,5-diF	4-SMe, 6-F	C14H10F3NO2S	313.30
B32	4,5-diF	4-SO_2Me, 6-F	C14H10F3NO4S	345.30
B33	3,4,5-triF	6-Me	C14H10F3NO2	281.24
B34	4,5-diF	4-Me, 6-F	C14H10F3NO2	281.24
B35	4-CO_2H	H	C14H11NO4	257.25
B36	H	4-CO_2H	C14H11NO4	257.25
B37	H	6-CO_2H	C14H11NO4	257.25
B38	6-CO_2H	H	C14H11NO4	257.25
B39	H	3-CF_3, 4-NH_2	C14H11F3N2O_2	296.25
B40	3-Me	2-NO_2, 5-Br	C14H11BrN2O4	351.16
B41	5-NO_2	2-F, 5-Me	C14H11FN2O4	290.25
B42	5-NO_2	2-Cl, 5-OMe	C14H11ClN2O5	322.71
B43	3-Br	4-Br, 6-CO_2H	C14H11Br2NO3	401.06
B44	2-CO_2H	H	C14H11NO4	257.25
B45	5-NO_2	2-Me, 4-Cl	C14H11ClN2O4	306.71
B46	H	2-Me, 3-NO_2	C14H12N2O4	272.26
B47	H	2-Me, 5-NO_2	C14H12N2O4	272.26
B48	3-Me	2-NO_2	C14H12N2O4	272.26
B49	5-NO_2	2-OMe	C14H12N2O5	288.26
B50	5-NO_2	3-OMe	C14H12N2O5	288.26
B51	4-OMe	2-NO2	C14H12N2O5	288.26
B52	H	2-Me, 4-NO_2	C14H12N2O5	288.26
B53	H	2-Me, 3-Cl	C14H12ClNO2	261.71
B54	4-Br	2-Me	C14H12BrNO2	306.16
B55	4-Cl	2-Me	C14H12ClNO2	261.71
B56	4-F	2-Me	C14H12FNO2	245.26
B57	4-Br	2-OMe	C14H12BrNO3	322.16
B58	4-F	2-OMe	C14H12FNO3	261.26
B59	4-Cl	3-OMe	C14H12ClNO3	277.71
B60	4-NO_2	3-OMe	C14H12N2O5	288.26
B61	4-NO_2	2-OMe	C14H12N2O5	288.26
B62	5-NO_2	2-OSO_2Me	C14H12N2O7S	352.32
B63	4-Cl	2-OMe	C14H12ClNO3	277.71
B64	H	4-Me	C14H13NO2	227.27
B65	H	3-Me	C14H13NO2	227.27
B66	H	4-OMe	C14H13NO3	243.26
B67	H	3-OMe	C14H13NO3	243.26
B68	H	3-OMe	C14H13NO3	243.26

B69	3-Me, 5-NH_2	H	C14H14N2O2	242.28
B70	4-OMe, 5-NH_2	H	C14H14N2O3	258.28
B71	4,5-diMe	4-CºCH	C15H8F3NO2	291.23
B72	4-Cl	2,6-diCO_2H	C15H10ClNO6	335.70
B73	5-CF_3	3-CO_2H	C15H10F3NO4	325.25
B74	H	2-$COCO_2H$, 5-Br	C15H10BrNO5	364.15
B75	5-CO_2H	4-CF_3	C15H10F3NO4	325.25
B76	5-CO_2H	2-CF_3	C15H10F3NO4	325.25
B77	3,5-diBr	2-CO_2Me	C15H11Br2NO4	429.07
B78	5-CO_2H	4-CO_2H	C15H11NO6	301.29
B79	4,5-diF	4-CO_2NHMe, 6-F	C15H11F3N2O3	324.26
B80	H	3-F, 5-CO_2Me	C15H12FNO4	289.26
B81	5-CO_2H	2-Me, 5-NO_2	C15H12N2O6	312.27
B82	4-Cl	2-CO2Me	C15H12ClNO4	305.72
B83	5-CO_2H	2-Cl, 5-OMe	C15H12ClNO5	321.72
B84	5-Cl	2-CH_2CO_2H	C15H12ClNO4	305.72
B85	5-NO_2	2-F, 5-NHCOMe	C15H12FN3O5	333.28
B86	4-Cl	2-CH_2CO_2H	C15H12ClNO4	305.72
B87	4-Br	2-CO_2Me	C15H12BrNO4	350.17
B88	5-CO_2H	2-Cl, 4-Me	C15H12ClNO4	305.72
B89	4-F	2-CO_2Me	C15H12FNO4	289.26
B90	2-CO_2H	4-SMe	C15H13NO4S	303.34
B91	H	2-COMe	C15H13NO3	255.28
B92	4-Cl	2,3-diMe	C15H14ClNO2	275.74
B93	H	2,3-diMe	C15H15NO2	241.29
B94	H	2,5-diMe	C15H15NO2	241.29
B95	5-OMe	2-OMe	C15H15NO4	273.29
B96	H	4-NMe_2	C15H16N2O2	256.31
B97	H	2,3-(4-pyridyl)	C16H12N2O2	264.29
B98	H	2,3-(3-pyridyl)	C16H12N2O2	264.29
B99	H	2,3-(5-pyridyl)	C16H12N2O2	264.29
B100	5-CF_3	2-CO_2Me	C16H12F3NO4	339.27
B101	4,5-diF	3,4-benzo	C17H11F2NO2	299.28
B102	4,5-diF	2,3-benzo	C17H11F2NO2	299.28
B103	3,4-benzo	H	C17H13NO2	263.29
B104	H	3,4-benzo	C17H13NO2	263.29
B105	H	2,3-benzo	C17H13NO2	263.29
B106	H	3-(4-pyridyl)	C18H14N2O2	290.32

B107	H	2-phenyl	C19H15NO2	289.34
B108	5-CO_2H	4-phenyl	C20H15NO4	333.35
B109	5-CO_2H	2-SPh	C20H15NO4S	365.41
B110	H	2-COPh	C20H15NO3	317.35
B112	5-aza	H	C12H10N2O2	214.22
B113	H	3-aza	C12H10N2O2	214.22
B114	H	4-aza	C12H10N2O2	214.22
B115	H	2-aza	C12H10N2O2	214.22
B115A	3-Me	2-Me	C15H15NO2	242.29
B116	4-OMe	2-Me	C15H15NO3	257.29
B116A	H	2-CH_2OMe	C15H15NO3	257.29
B117	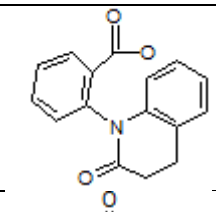		C16H13NO3	267.29
B118	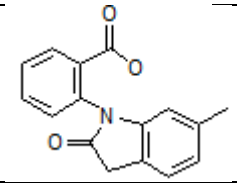		C16H13NO3	267.29
Compounds B119 to B136 are 2-phenoxybenzoic acid derivatives			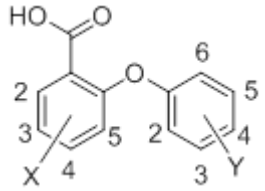	
B119	H	2-CN	C14H9NO3	239.23
B120	4-NO_2	2-Me	C14H11NO5	273.25
B121	3-NO_2	2-Me	C14H11NO5	273.25
B122	H	2-Me, 5-NO_2	C14H11NO5	273.25
B123	H	2-Me, 3-NO_2	C14H11NO5	273.25
B124	H	2-Me, 5-Cl	C14H11ClO3	262.7
B125	H	2-Me, 3-Cl	C14H11ClO3	262.7
B126	3-Cl	2-Me	C14H11ClO3	262.7
B127	5-Cl	2-Me	C14H11ClO3	262.7
B128	5-NO_2	2-OMe	C14H11NO6	289.25
B129	4-Me	H	C14H12O3	228.25
B130	H	2-Me	C14H12O3	228.25
B131	H	3-Me	C14H12O3	228.25
B132	H	4-Me	C14H12O3	228.25

B133	H	2-OMe	C14H12O4	224.25
B133A	H	2-Et	C15H14O3	242.28
B134	3-OMe	2-Me	C15H14O4	258.28
B135	4-OMe	2-Me	C15H14O5	274.28
B136	5-OMe	2-OMe	C15H14O5	274.28

Table S3. List of compounds used for SAR studies.

		Residues lining the internal cavity																
	Docking Score (kcal/mol)	**Ser 96**	**His 246**	**Ser 219**	**Phe 194**	**Phe 135**	**His 218**	**Phe 158**	**Val 143**	**Trp 154**	**Phe 27**	**Met 147**	**Ser 190**	**Val 193**	**Val 97**	**Phe 125**	**Phe 144**	**Ile 140**	**Ala 162**
DAD2	-10.6																		
DAD2$_{Phe27Val}$	-8.0										Val								
Z. mays	-10						Val	Tyr					Cys						
S. bicolor	-10						Val	Tyr					Cys						
P. persica	-9.9						Val												
A. lyrata	-9.9						Val												
V. vinifera	-9.9						Val							Ile					
R. communis	-9.9						Val												
P. trichocarpa_1	-9.9						Val												
M. truncatula	-9.8						Met								Ile				
M. grandiflora	-9.7						Val												
A. trichopoda	-9.7						Val						Cys	Ile					
B. distachyon	-9.7						Val	Tyr					Cys						
***O. sativa* (OsD14)**	-9.7						Val	Tyr					Cys						
C. sativus	-9.5						Val							Ile					
***A. thaliana* (AtD14)**	-9.5						Val												
A. coerulea	-9.2*						Cys		Leu				Cys						
S. italica	-9.1*						Val	Tyr					Cys						
M. esculenta	-8.6						Val				Val								
M. guttatus	-8.4*						Val		Phe										
P. trichocarpa_2	-8.3						Val				Val								

*Best docking solutions have pose different from tolfenamic acid in DAD2 structure. Scores shown are from the second docking solutions, whose poses are similar to tolfenamic acid in DAD2 structure.

Table S4. Autodock Vina docking score for tolfenamic acid in models of D14 orthologues. The models are ranked by decreasing order of the tolefenamic acid docking score (binding affinity) value. Protein accession numbers for D14 orthologues are JQ654486 (*petunia hybrid*a), XM_008662207 (*Zea mays*), XM_002468271 (*Sorghum bicolor*), XM_007222936 (*Prunus persica*), XM_002882278 (*Arabidopsis lyrata*), XM_002281331 (*Vitis vinifera*), XM_002510055(*Ricinus communis*), XM_002320654 (*Populus trichocarpa_1*), XM_003589038 (*Medicago truncatula*), WBOD-2007195 (*Magnolia grandiflora*), XM_006849255 (*Amborella trichopoda*), XM_003558507 (*Brachypodium distachyon*), XM_015775914 (*Oryza sativa ssp. Japonica*), XM_004142842 (*Cucumis sativus*), AY064145 (*Arabidopsis thaliana*), Aqcoe6G293700 (*Aquilegia coerulea*), XM_004985235 (*Setaria italica*), Manes18G046100 (*Manihot esculenta*), XM_012989321 (*Mimulus guttatus*), XM_002302373 (*Populus trichocarpa_2*).

Supplementary Figures

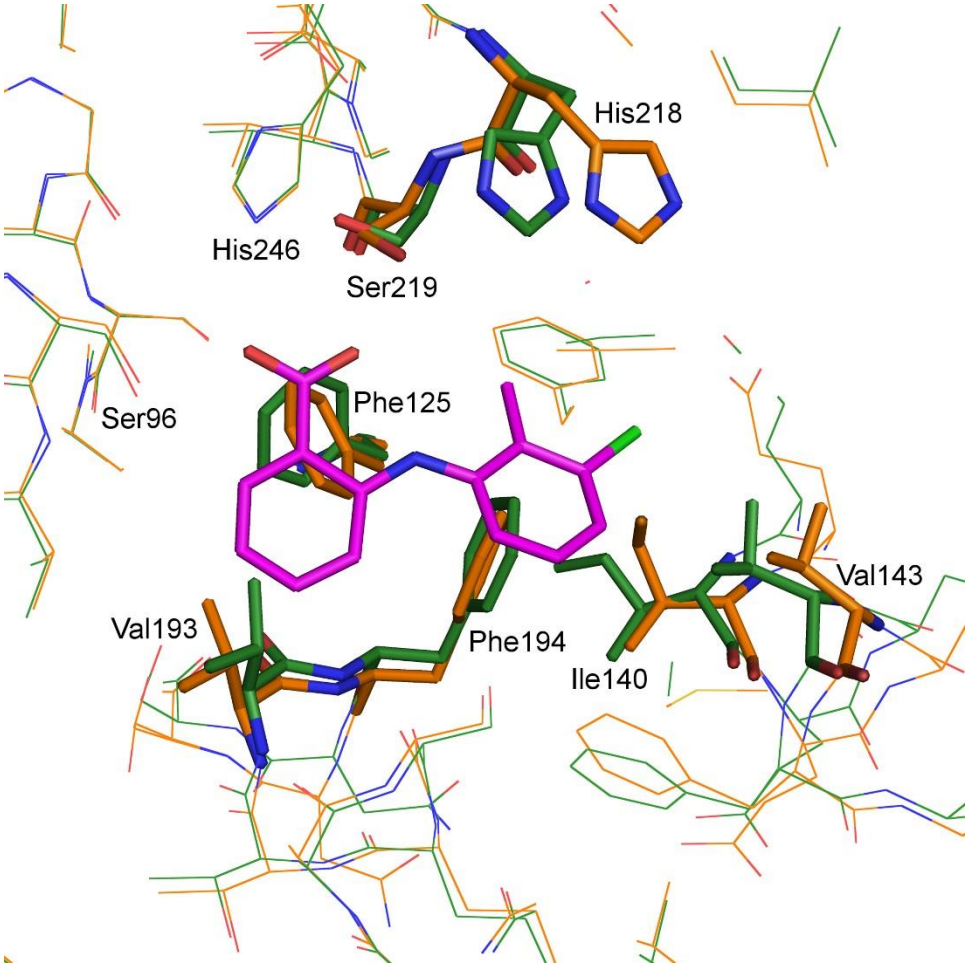

Figure S1. Structural comparisons. Structural superimposition between the apo (green) and tolfenamic acid-bound (orange) structures. Residues undergoing conformational changes around tolfenamic acid are drawn in stick mode and labelled.

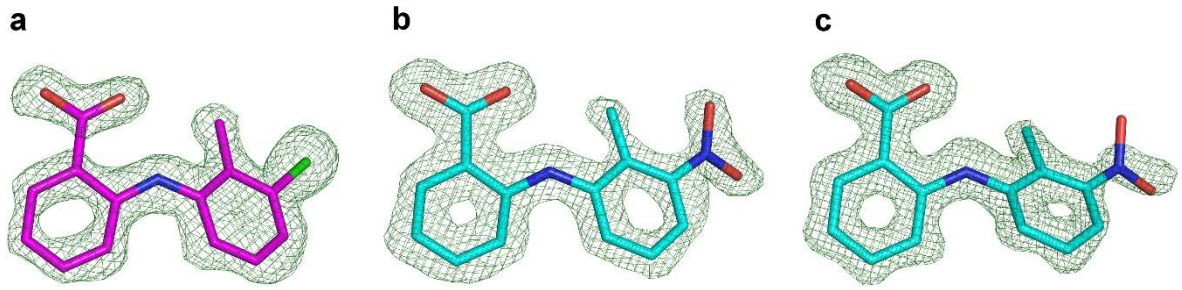

Figure S2. Omit maps for the DAD2/tolfenamic acid (**a**), DAD2/MNAB (**b**) and OsD14/MNAB (**c**) structures. To generate the omit maps, bound compounds were removed from the final PDB models. After 10 cycle of restrained refinement in refmac, the sigmaA-weighted difference maps (omit maps) were calculated. Omit maps contoured at 3 σ are shown in green, together with the bound compounds of the final PDB models.

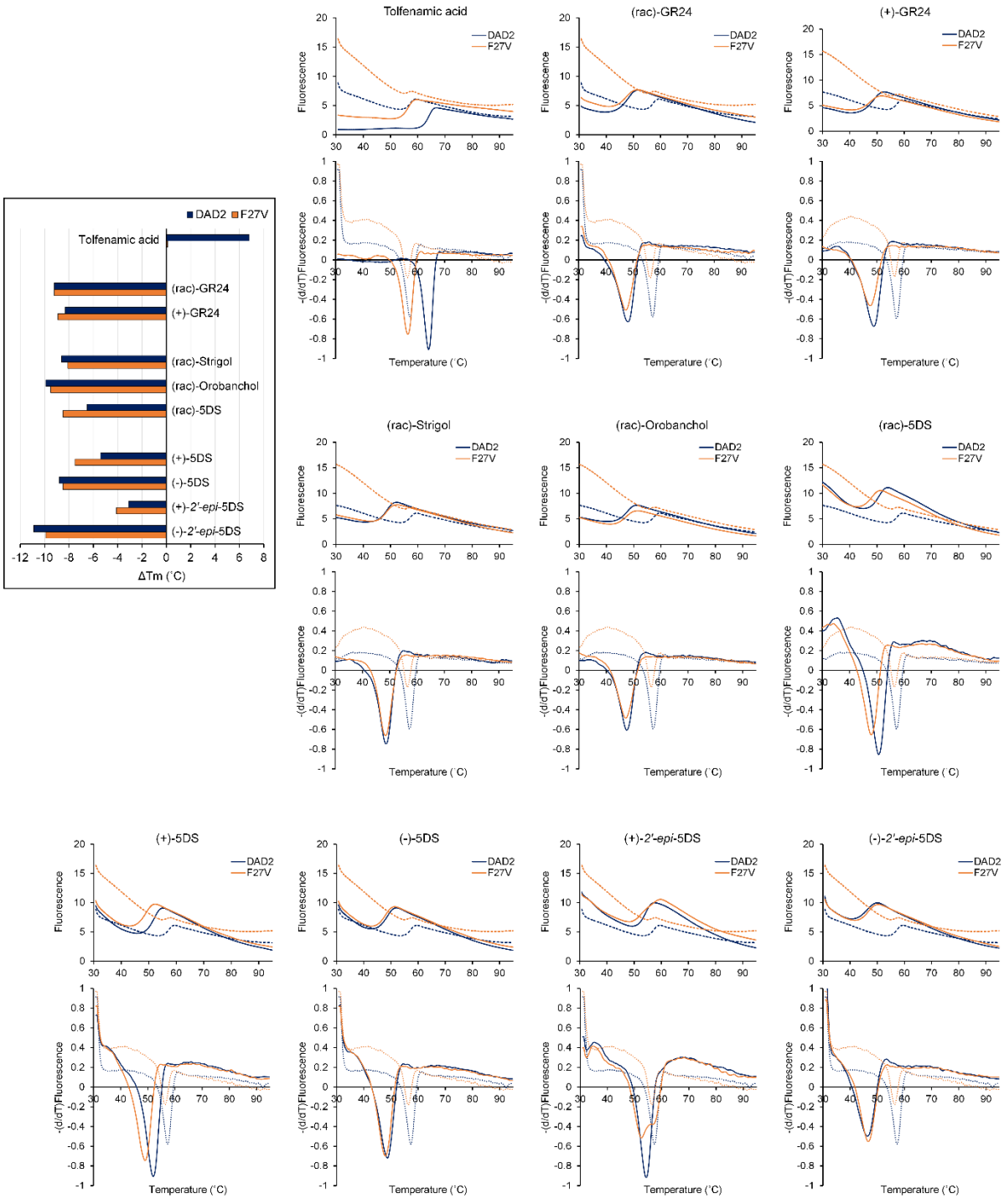

Figure S3. DSF assay of DAD2 and DAD2$_{Phe27Val}$ (F27V). The insert shows a summary of melting shifts observed for DAD2 and DAD2$_{Phe27Val}$ (F27V) in presence of tolfenamic acid and strigolactone compounds. Experimental melting curves and derivatives of melting curves are shown for each individual compound (dotted lines are DMSO controls while solid lines are in presence of compounds). All experiments were performed in triplicates.

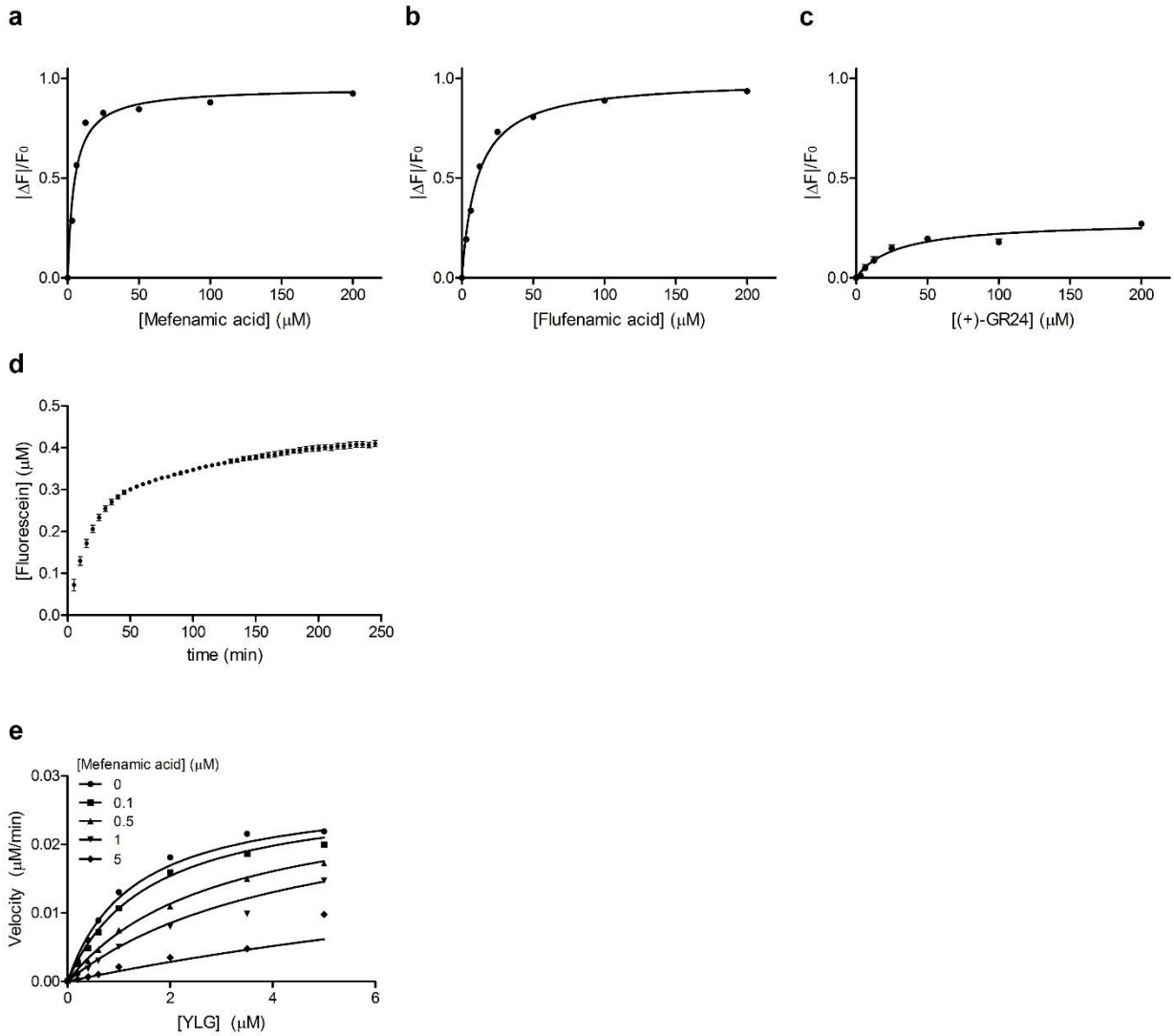

Figure S4. DAD2 binding and kinetics. (**a**) (**b**) (**c**) Binding curves of mefenamic acid, flufenamic acid and (+)-GR24, respectively, to DAD2 using intrinsic fluorescence experiments. Each data point is the mean ± s.e.m. of three technical replicates. (**d**) Progress curve of YLG hydrolysis (1 μM) by DAD2 (0.34 μM) over 4 hours. Each data point is the mean ± s.e.m. of three technical replicates. (**e**) YLG hydrolysis competition assays using mefenamic acid. Each data point is the average of 3 technical replicates. All the individual replicates for each compound concentration were included during the non-linear global fit analysis using mixed-inhibition model.

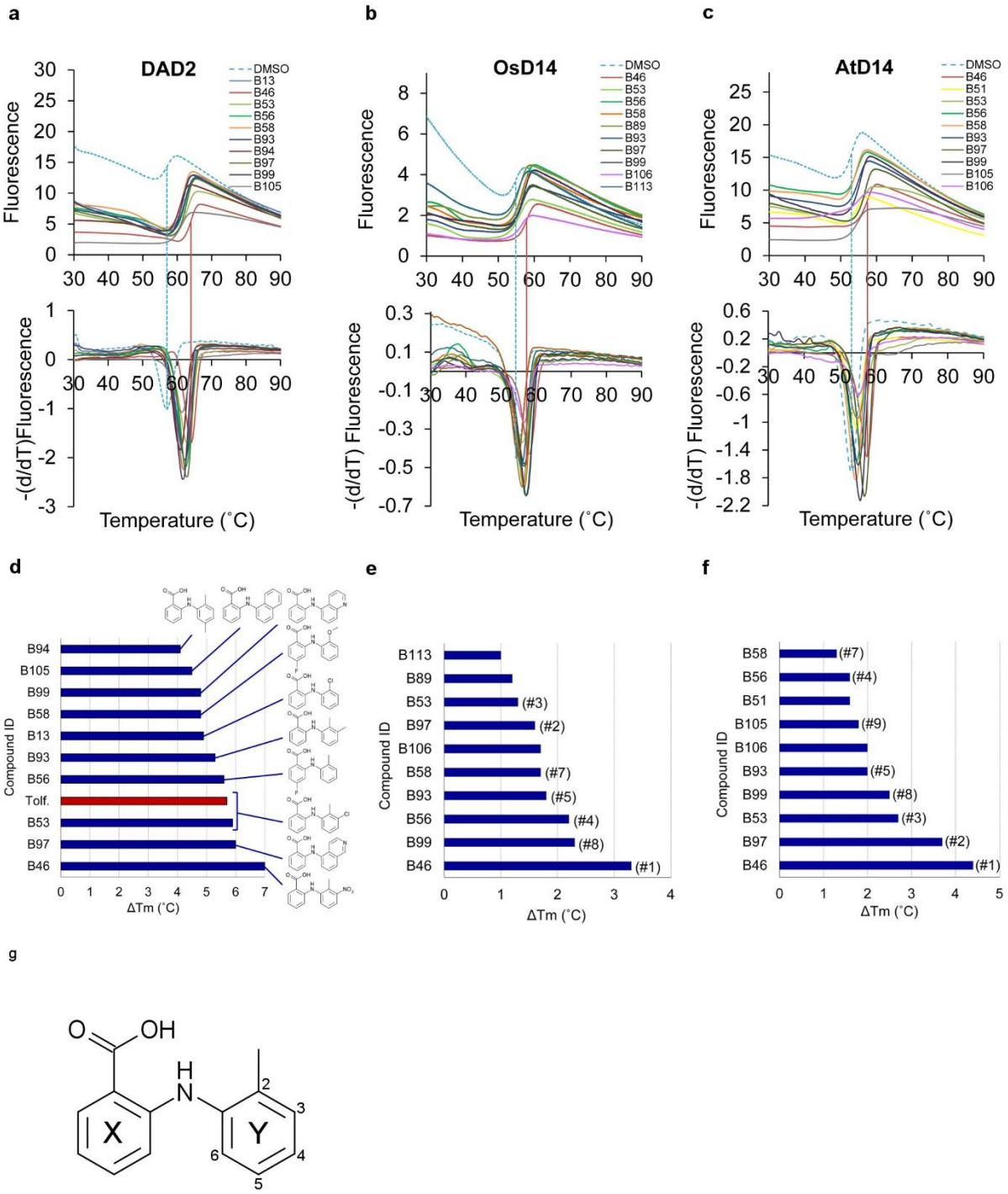

Figure S5. SAR study. Experimental melting curves and derivatives of the melting curves for DAD2 (**a**), OsD14 (**b**) and AtD14 (**d**) in presence of the top ten compounds. The dotted and plain vertical lines corresponds to the melting temperatures of DAD2, OsD14 and AtD14 in presence of DMSO and of the best compound, B46 (MNAB), respectively. (**d**), (**e**) and (**f**) Histograms of the ten largest melting temperature shifts observed for DAD2, OsD14 and AtD14, respectively. In (**e**) and (**f**) compounds that also trigger a shift in DAD2's melting temperature are indicated by a number at the right side of each bar, the number referring to the position of this compound within DAD2's top ten list (**d**). (**g**) N-(2-Methylphenyl)anthranilic acid represents the core pharmacophore, as determined from the SAR experiments.

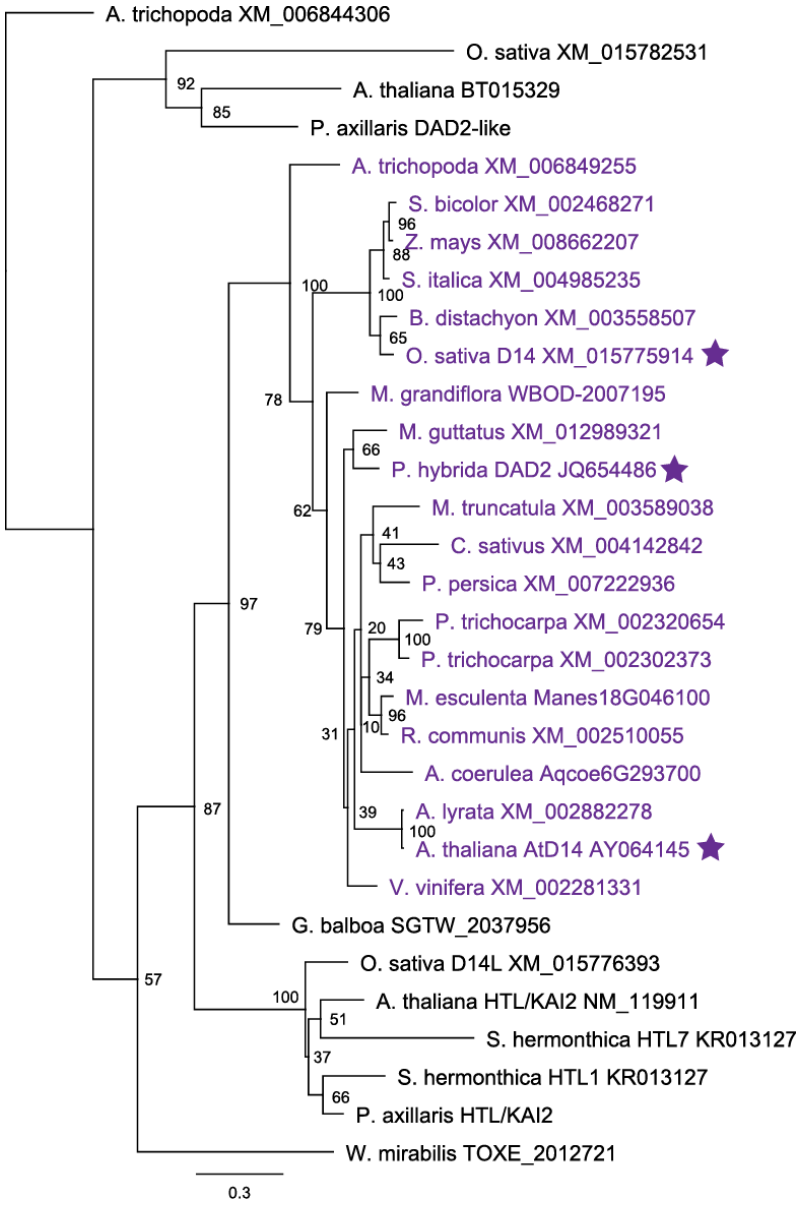

Figure S6. DAD2 phylogenetic analysis. A phylogenetic tree of a selection of the α/β fold hydrolases related to DAD2. Proteins with similarity to DAD2 were identified using BLAST searches against the *Petunia axillaris* genome (https://solgenomics.net/); the 1000 plants project (https://sites.google.com/a/ualberta.ca/onekp/) *G. balboa*, *W. mirabilis*, and *M. grandiflora*; Phytozome (https://phytozome.jgi.doe.gov) *A. coerulea* and *M. esculenta*; and the remaining sequences from the NCBI databases. The protein sequences were aligned using Geneious Align as implemented in Geneious R8 and manually corrected. The alignment is available in Supplemental data file 3 in nexus format. A maximum likelihood tree was drawn using RAxML and the topology support was calculated with 1000 bootstrap replicates and manually rooted on the *A. trichopoda* XM_006844306 node. The proteins included in the modelling and docking analysis are shown in purple. The three proteins marked with stars were expressed and proteins analysed biochemically.

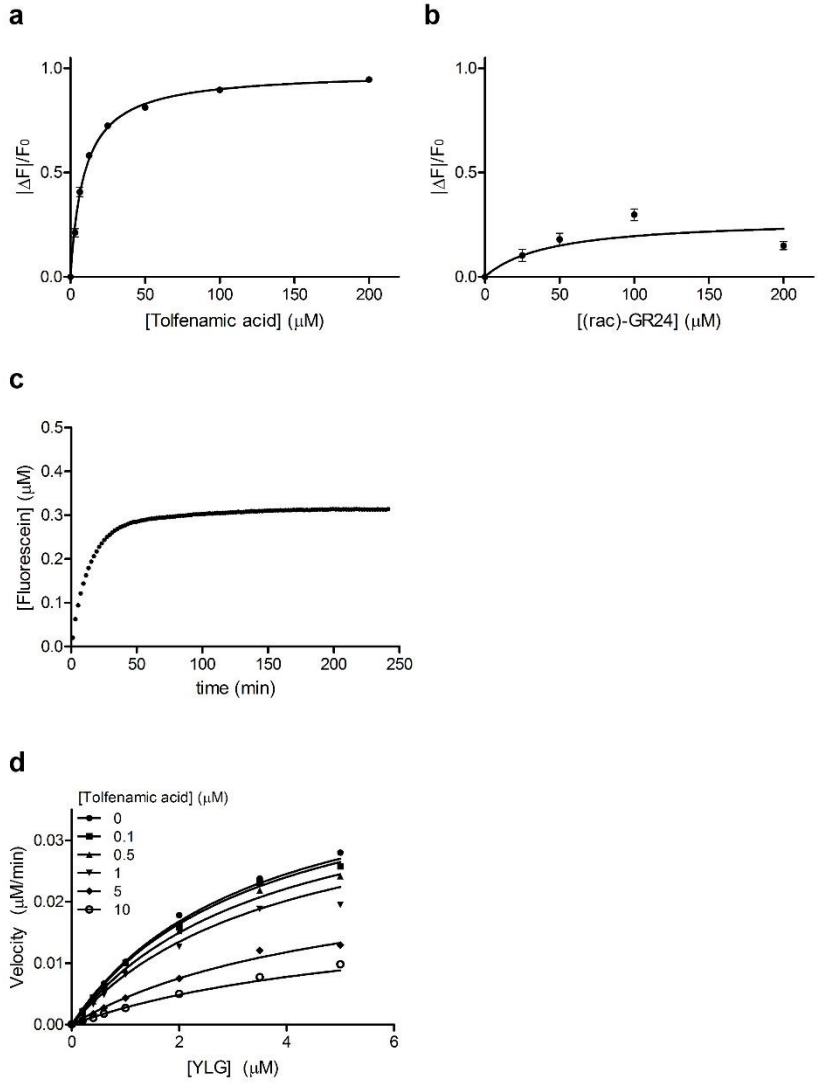

Figure S7. OsD14 binding and kinetics. (**a**) (**b**) Binding curves of tolfenamic acid and (rac)-GR24, respectively, to OsD14 using intrinsic fluorescence experiments. Each data point is the mean ± s.e.m. of three technical replicates. (**d**) Progress curve of YLG hydrolysis (1 μM) by OsD14 (0.34 μM) over 4 hours. Each data point is the mean ± s.e.m. of three technical replicates. (**e**) YLG hydrolysis competition assays using tolfenamic acid. Each data point is the average of 3 technical replicates. All the individual replicates for each compound concentration were included during the non-linear global fit analysis using mixed-inhibition model.

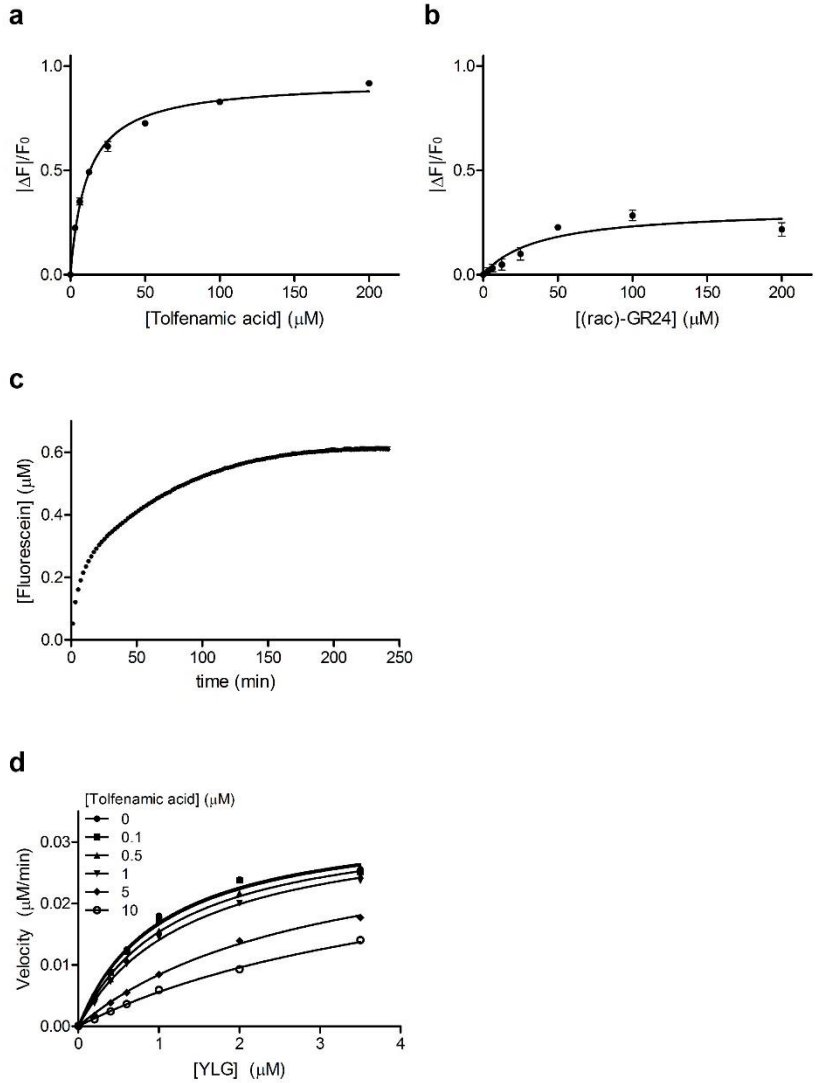

Figure S8. AtD14 binding and kinetics. (**a**) (**b**) Binding curves of tolfenamic acid and (rac)-GR24, respectively, to AtD14 using intrinsinc fluorescence experiments. Each data point is the mean ± s.e.m. of three technical replicates. (**d**) Progress curve of YLG hydrolysis (1 μM) by AtD14 (0.34 μM) over 4 hours. Each data point is the mean ± s.e.m. of three technical replicates. (**e**) YLG hydrolysis competition assays using tolfenamic acid. Each data point is the average of 3 technical replicates. All the individual replicates for each compound concentration were included during the non-linear global fit analysis using mixed-inhibition model.

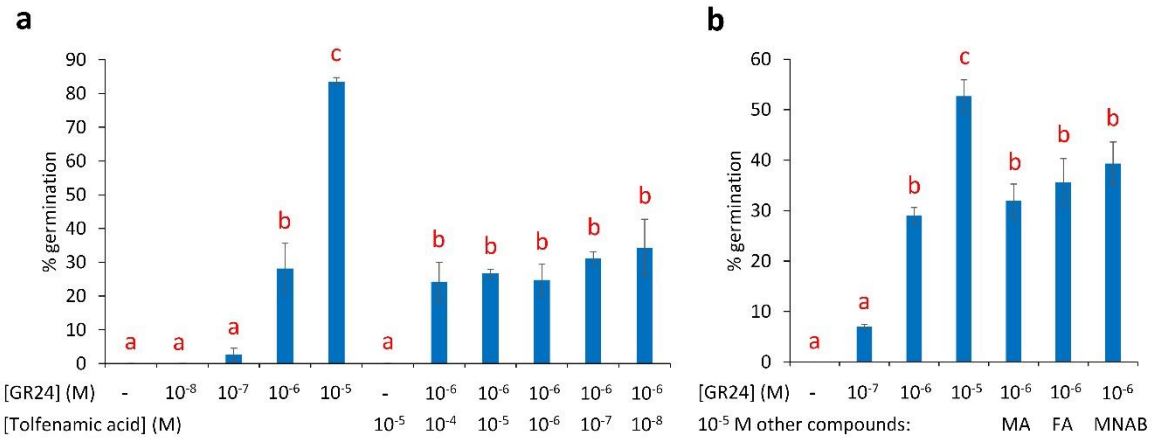

Figure S9. Effects of compounds on germination of *Orobanche minor* seed. (**a**) Treatments had different concentrations of GR24 and tolfenamic acid; n=3 replicates each containing 48-116 seed, data shown are means ± s.e.m. (**b**) treatments had GR24 and either mefenamic acid (MA), flufenamic acid (FA) or 2-(2'-methyl-3'-nitroanilino)benzoic acid (MNAB); n=3 replicates each containing 34-120 seed, data shown are means ± s.e.m. Statistical tests of differences between treatments were calculated by ANOVA, values with the same lower case identifier (in red, within each experiment) are not significantly different from each other (P=0.01).

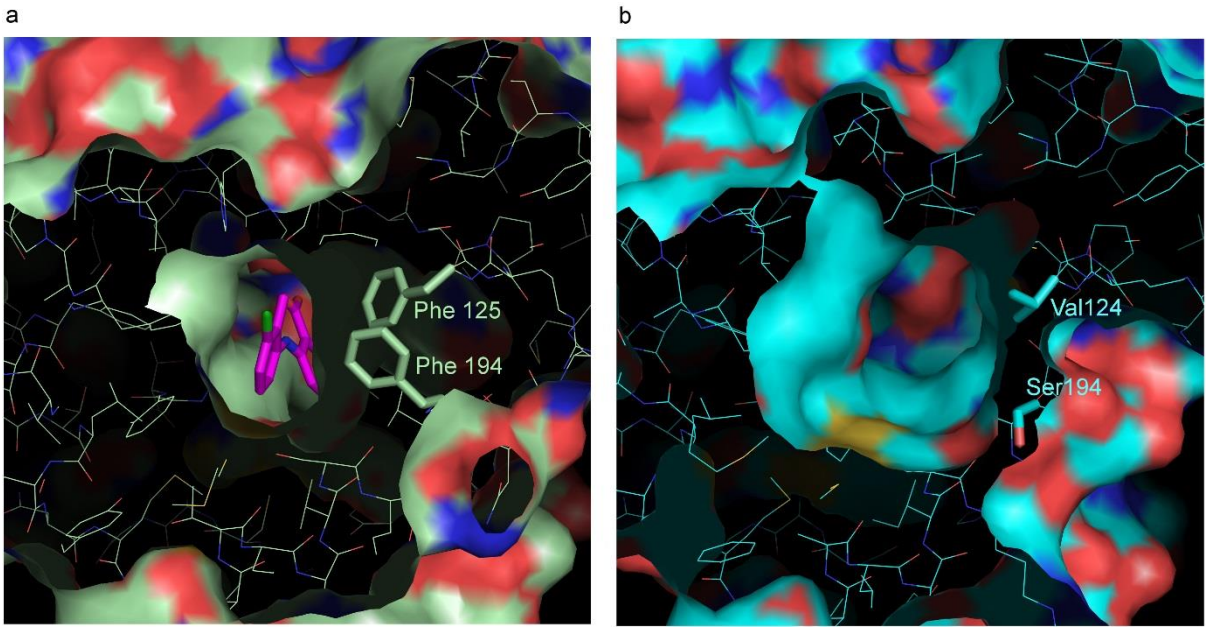

Figure S10. Comparisons of the internal cavities of DAD2 and ShHTL5. (**a**) Surface representation of DAD2 showing its internal cavity, with bound tolfenamic acid drawn in pink. Phe125 and Phe194 lining the right side of the cavity are highlighted in stick mode. (**b**) Surface representation of ShHTL5 (PDB 5CBK) showing its internal cavity drawn in the same orientation as DAD2. The absence of Phe125 and Phe194, replaced by Val124 and Ser194, respectively, creates a much larger cavity at the right hand side of the position where tolfenamic acid is bound in the DAD2 structure.

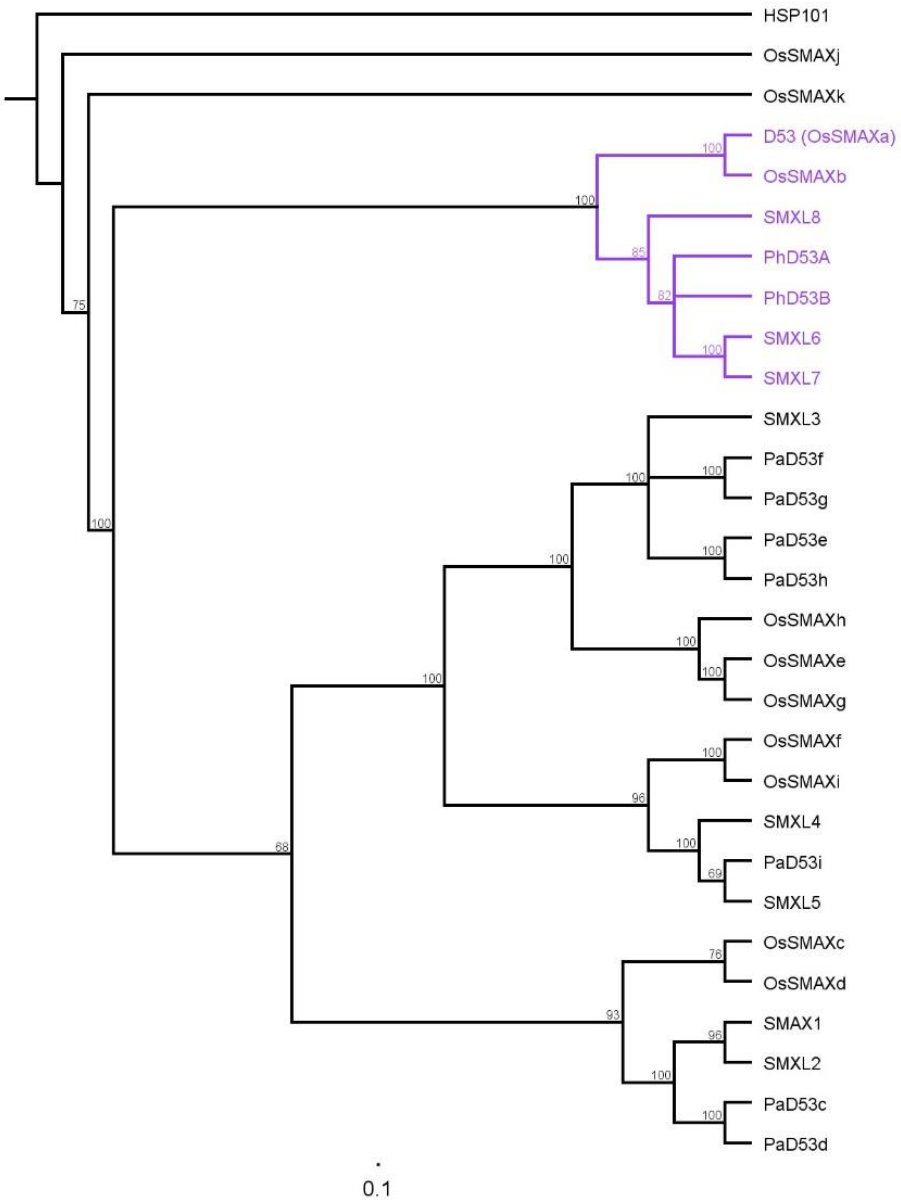

Figure S11. D53 Phylogenetic analysis. A phylogenetic tree of the petunia, rice and Arabidopsis D53 proteins. Proteins with sequence similarity to the D53 protein from rice were identified using iterative BLAST searches against the petunia genome (https://solgenomics.net/), the rice genome (http://rice.plantbiology.msu.edu/) and the Arabidopsis genome (https://www.arabidopsis.org/). The proteins identified are available in Supplemental data file 1 with the names we have assigned and the original accession numbers from the relevant databases. An alignment was calculated using Geneious Align as implemented in Geneious R8 and manually corrected and is available in Supplemental data file 2 in nexus format. A maximum likelihood tree was drawn using RAxML and the topology support was calculated with 1000 bootstrap replicates and manually rooted on the HSP101 node. The clade containing the original rice D53 has been highlighted in magenta.

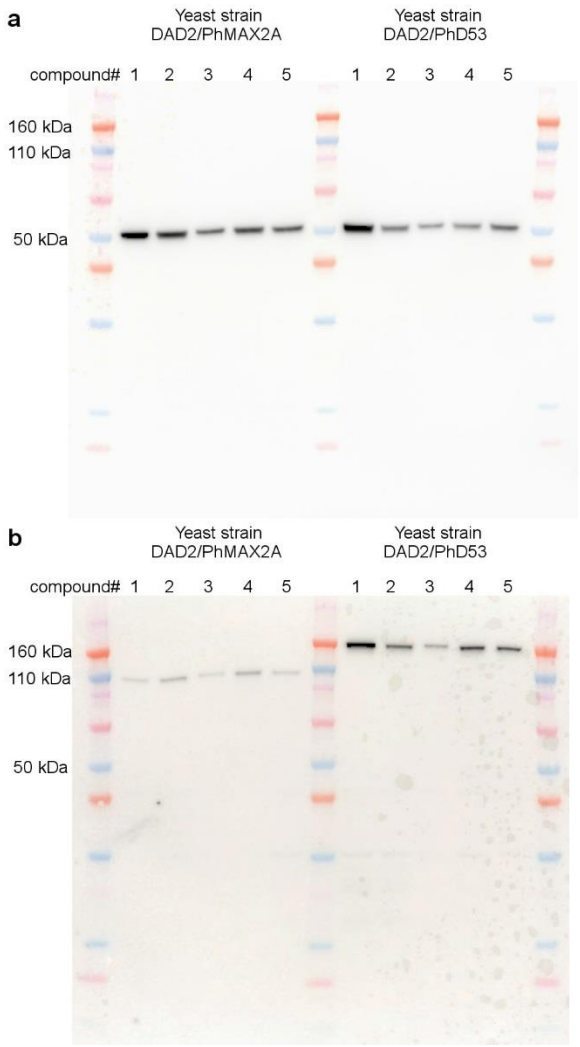

Figure S12. Western blot controls for expression of proteins in yeast. (a) Detection of the binding domain of GAL4 (fused to DAD2) using the Santa Cruz GAL-TA (C10) primary antibody. (b) Detection of the activation domain of GAL4 (fused to PhMAX2A or PhD53) using the Santa Cruz GAL4 (RK5C1) primary antibody. In both cases, the secondary antibody was Goat Anti-Mouse IgG (H + L)-HRP conjugate (Biorad #1706516). Yeast cells were grown in the presence of the following compounds, as indicated: 1-DMSO ; 2-(rac)GR24 5 µM ; 3-Tolfenamic acid 50 µM ; 4-Mefenamic acid 50 µM and 5-Flufenamic acid 50 µM.